Solution Structure of the N-Terminal EGF-like Domain from Human Factor VII[†,‡]

Andreas Muranyi,*[,§] Bryan E. Finn,[§] Garry P. Gippert,[§] Sture Forsén,[§] Johan Stenflo,[||] and Torbjörn Drakenberg[§]

Physical Chemistry 2, Lund University, PO Box 124, S-221 00 Lund, Sweden, and Clinical Chemistry, Lund University, University Hospital, S-205 02 Malmö, Sweden

Received March 6, 1998; Revised Manuscript Received May 11, 1998

ABSTRACT: Blood coagulation is initiated by Ca^{2+}-dependent binding of coagulation factor VIIa (FVIIa) to its cofactor, tissue factor (TF). The TF:FVIIa complex activates factors IX and X, ultimately leading to the formation of thrombin and the coagulation of blood. FVII consists of an N-terminal γ-carboxyglutamic-acid-containing (Gla) domain followed by two epidermal growth factor (EGF) like domains, the first of which can bind one Ca^{2+} ion ($K_d \approx 150$ μM) and a C-terminal serine protease domain. Using ^{1}H nuclear magnetic resonance spectroscopy, we have determined the solution structure of a synthetic N-terminal EGF-like domain (EGF1) of human FVII (residues 45−85) in the absence of Ca^{2+}. A comparison of this structure of apo EGF1 with the Ca^{2+}-bound EGF1 in the complex of FVIIa and TF [Banner, D. W., et al. (1996) *Nature 380,* 41−46] suggests that the structural changes in the EGF1 domain upon Ca^{2+} binding are minor and are concentrated near the Ca^{2+}-binding site, which is facing away from the TF interaction surface. Amino acid side chains that are crucial for the binding of FVII to TF show a similar conformation in both structures and are therefore unlikely to directly influence the Ca^{2+}-dependent binding of FVII to TF. As Ca^{2+} binding to EGF1 does not lead to a conformational change in the residues constituting the interaction surface for binding to TF, our results are consistent with the idea that the altered orientation between the Gla and EGF1 domains that result from Ca^{2+} binding is responsible for the increased affinity of FVII/FVIIa for TF.

Coagulation factor VII (FVII)[1] is a 50 kD (406 amino acid) vitamin K-dependent glycoprotein important in the initiation of the blood coagulation cascade (*1*−*3*). It circulates in an inactive zymogen form in blood plasma at a concentration of approximately 0.5 mg/L (*4*). Simultaneously, 4 μg/L of the activated protease form FVIIa circulates in the blood (*5*−*7*). The free enzyme is virtually inactive against its physiological substrate. FVII, like coagulation factors IX (FIX) and X (FX) and protein C, consists of an N-terminal γ-carboxyglutamic acid containing (Gla) domain followed by two domains homologous to epidermal growth factor (EGF-like domains) and a C-terminal serine protease domain (Figure 1).

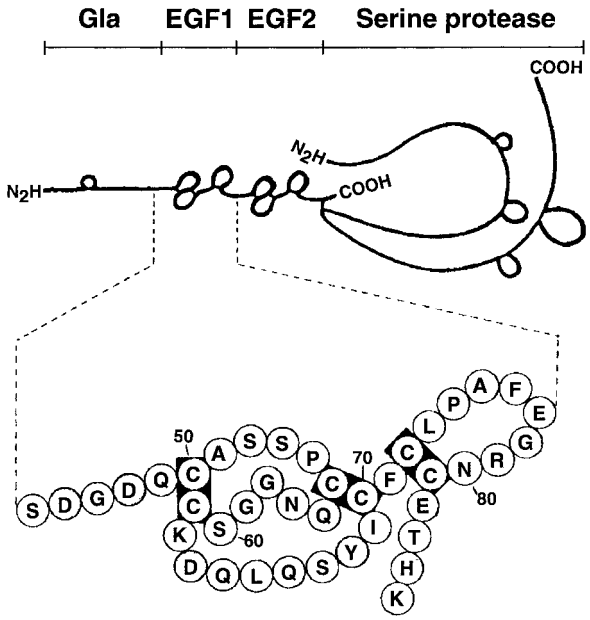

FIGURE 1: FVII contains an N-terminal Gla domain followed by two EGF-like domains and a serine protease domain. We have determined the tertiary structure of the N-terminal EGF-like domain (EGF1) consisting of residues 45−85.

Tissue factor (TF) is an integral membrane glycoprotein (*8*, *9*). It has an extracellular part that consists of two β-strand modules of C2 immunoglobulin-like topology (*10*,

† This work was supported by grants from the Swedish Foundation of Strategic Research, the Swedish Medical Research Council and the European Union Biotechnology Program (Contract BIO4-CT96-0662).

‡ Coordinates for the final ensemble of 23 structures have been deposited in the Brookhaven Protein Data Bank under the file name 1bf9.

* To whom correspondence should be addressed. E-mail: andreas.muranyi@fkem2.lth.se.

§ Physical Chemistry.

|| Clinical Chemistry.

[1] Abbreviations: FVII, coagulation factor VII (zymogen); TF, tissue factor; FVIIa, activated coagulation factor VII; FIX, coagulation factor IX; FX, coagulation factor X; Gla, γ-carboxyglutamic acid; EGF, epidermal growth factor; FIXa, activated coagulation factor IX; FXa, activated coagulation factor X; EGF1, N-terminal EGF-like domain; K_d, dissociation constant; Fmoc, *N*-(9-florenyl)methoxycarbonyl; NMR, nuclear magnetic resonance; COSY, two-dimensional correlation spectroscopy; 2Q, two-dimensional double quantum; TOCSY, two-dimensional total correlation spectroscopy; NOESY, two-dimensional nuclear Overhauser enhancement spectroscopy; 2D, two-dimensional; TPPI, time-proportional phase-incrementation frequency discrimination; NOE, nuclear Overhauser enhancement; PDB, Protein Data Bank; TGF-α, transforming growth factor α; hEGF, human epidermal growth factor; u-PA, urokinase-type plasminogen activator; t-PA, tissue-type plasminogen activator.

S0006-2960(98)00522-4 CCC: $15.00
Published on Web 07/03/1998

11). Under normal circumstances, TF is located in the blood-vessel adventitia. Upon injury and vessel wall rupture, TF becomes exposed to blood, and FVII/FVIIa binds to TF in a Ca^{2+}-dependent manner forming a complex on the phospholipid membrane. Upon TF binding, FVII is rapidly activated to FVIIa by proteolytic cleavage between Arg^{152} and Ile^{153} leaving a two-chained molecule with an N-terminal light chain of 152 amino acids and a C-terminal heavy chain of 254 amino acids, connected by a disulfide bridge between Cys^{135} and Cys^{262} (*12, 13*). FVIIa with TF as cofactor activates FIX and FX, ultimately leading to the formation of thrombin and the coagulation of blood (*14, 15*). Several biochemical studies, reviewed by Martin et al. (*16*), imply that the N-terminal EGF domain (FVII EGF1) is important for the binding of FVII to TF. In the crystal structure of the TF:FVIIa complex, all four domains of FVIIa are shown to contact TF, the largest part of the intermolecular contact area being on FVII EGF1 (*17*). Analysis of the TF:FVIIa complex structure and biochemical studies suggest that EGF1 is primarily responsible for tethering FVII to TF, while the cofactor function of TF is conveyed to the serine protease domain which undergoes a conformational change upon binding, dramatically increasing the enzymatic activity (*18*−*21*).

FVII contains seven low-affinity ($K_d \approx 1$ mM) Ca^{2+}-binding sites in the Gla domain and two high-affinity ($K_d \approx 150$ μM) Ca^{2+} binding sites, one located in EGF1 and the other one in the serine protease domain (*17, 22, 23*). Ca^{2+}-binding to the low-affinity sites in the Gla domain enables binding of FVII to anionic phospholipid membranes, while the high-affinity sites are associated with amidolytic activity and binding affinity to TF (*24, 25*). The Ca^{2+}-ion in EGF1 is coordinated by six oxygen atoms from five residues in EGF1 and one oxygen atom in a water molecule (*17, 26*). Out of the Ca^{2+}-ligating residues, only Gln^{64} has direct contact to tissue factor in the complex. When site-directed mutagenesis was employed to abolish the Ca^{2+} binding of EGF1, the mutated protein had a 25-fold higher K_d than wild-type FVII for binding to TF. Further, the amidolytic activity was 2−3 times lower for the mutant compared with the wild-type, in the presence as well as in the absence of the soluble form of the cofactor (*25*). Other mutational studies have shown similar results (*19*). Previous structural studies of homologous domains (*27*) as well as mutational studies of FVIIa (*19*) have attributed the Ca^{2+} dependence of the function, which in the case of FVIIa is TF binding and amidolytic activity, to a rearrangement and stabilization of the relative orientation of EGF1 and the Gla domain rather than a local conformational change within the EGF domain.

Human plasma FVII has two O-glycosylated serine residues in the N-terminal EGF-like domain and two N-glycosylated aspargines in the serine protease domain (*28, 29*). The function of these glycosylations is unknown.

EGF-like domains are found in a wide variety of extracellular proteins exhibiting diverse biological functions (*30*−*33*). In these proteins, the EGF-like domains are often involved in protein−protein interactions. EGF-like domains usually contain 40−50 residues, including six conserved cysteines forming three disulfide bridges paired 1−3, 2−4, and 5−6. The main feature of the fold is a central two-stranded antiparallel β-sheet connected to the N-terminal part of the domain by two of the disulfide bridges. The third disulfide bridge connects the central part of the molecule to the C-terminal part which also contains a short stretch of two-stranded antiparallel β-sheet.

In the present study, we examine the role of Ca^{2+} binding to FVII EGF1 by determining the structure of the Ca^{2+}-free form of the isolated domain and comparing the results with the EGF1 domain, with one Ca^{2+} ion bound, in the structure of the TF:FVIIa complex.

MATERIAL AND METHODS

Protein Synthesis. The N-terminal EGF module of human factor VII, residues 45−85 (Figure 1), was synthesized using Fmoc chemistry on a Milligen/Biosearch 9050 peptide synthesizer. The peptide was simultaneously cleaved from the resin and deprotected by treatment with 95% trifluoroacetic acid and 5% scavenger mixture (equal volumes of phenol and ethanedithiol), then extracted with ether and evaporated to dryness. The peptide was reduced and reoxidized overnight at 16 °C in a refolding buffer consisting of 0.1 M Tris-HCl, pH 8.3, 3 mM cysteine, 0.3 mM cystine, and 1 mM EDTA (*34*). The reoxidized material was purified by reversed-phase high-performance liquid chromatography (Kromasil 5, C8, 100A, 250 × 21 mm) using a 15−40% acetonitrile gradient in 0.1% trifluoroacetic acid over 60 min, after which the product was lyophilized.

Sample Preparation. A total of 4.4 mg of the protein was dissolved in 250 μL of 90% H_2O/10% D_2O, yielding a protein concentration of 3.2 mM (sample 1). A second sample of the same protein was prepared in a similar fashion, this time, however, to 320 μL of protein solution with a protein concentration of 2.2 mM (sample 2). A D_2O sample was prepared by performing four cycles of lyophilizing of sample 2 and redissolving it in 99.998% D_2O (sample 3). The pH was adjusted to 5.56 by addition of microliter amounts of NaOH and HCl (or NaOD and DCl for the D_2O experiments).

NMR Experiments. Homonuclear 2D ^1H NMR spectra were acquired using standard pulse sequences and phase cycling on two spectrometers; a GE Omega NMR spectrometer operating at a proton frequency of 500.11 MHz and a Varian Unity Plus NMR spectrometer operating at 599.89 MHz.

At 500 MHz using sample 1, COSY (*35*), 2Q (*36*), TOCSY (*37*), and NOESY (*38*) spectra used for resonance assignment were acquired at a temperature of 25 °C. In addition COSY and NOESY spectra were acquired at 15 and 35 °C to resolve ambiguities in case of resonance overlap. With sample 2 at 600 MHz and 25 °C, a high-resolution COSY spectrum for measuring $^3J_{H^N-H^\alpha}$ coupling constants and a TOCSY spectrum were acquired. Sample 2 was freeze-dried and redissolved in D_2O and a series of one-dimensional experiments was acquired to monitor the exchange of amide protons. On the same instrument two series of NOESY spectra with mixing times of 20, 40, 80, 130, and 200 ms were acquired using sample 2 (90% H_2O/10% D_2O) and sample 3 (D_2O).

The 2D spectra were acquired using a standard protocol of 512 t_1 increments collected using States-TPPI, with 2048 complex data points in the t_2 domain. The high-resolution COSY spectrum was recorded with 4096 complex data points in the acquisition (t_2) dimension. In the TOCSY and NOESY

experiments, 96 scans were collected in each spectrum and, in the COSY, 64 scans were acquired. The carrier frequency was set on the water resonance, which was suppressed using a selective pulse for presaturation.

Zero-filling in the evolution (t_1) dimension provided final 2D spectra of 1024 × 2048 real points, except in the high-resolution COSY spectrum, which after processing consisted of a 1024 × 16 384 matrix.

For all experiments, the spectral width in both dimensions was set to 7692 Hz on the 600 MHz and 6410 Hz on the 500 MHz spectrometer, except for the 2Q experiment where the spectral width was 6410 Hz in the acquisition dimension and 10 000 Hz in the evolution dimension.

Data Processing and Analysis. All spectra were processed and analyzed on Silicon Graphics and Sun workstations using the program FELIX 95 (Molecular Simulations Inc).

Identification of Spin Systems and Sequential Assignment. Sequence-specific resonance assignments were made using standard methods (*39*) by first identifying amino acid spin systems from cross-peak patterns in COSY, TOCSY, and 2Q spectra, followed by sequential assignment using cross-peaks in the 200 ms NOESY spectrum. For spin system identification and sequential resonance assignment, we used a side chain directed approach closely resembling the approach presented by Chazin et al. (*40, 41*). Secondary structure elements were assigned based on the observation of protected amide protons, $^3J_{H^N-H^\alpha}$ couplings and regular patterns of NOE peaks (*39*).

Assignment of Remaining NOE Cross-Peaks, Experimental Restraints and Structure Calculation. As far as possible, the remaining medium- and long-range NOE cross-peaks were assigned based on the chemical shifts. In cases of shift degeneracy, up to two assignment alternatives in each dimension were retained. Volumes were measured, and build-up curves were determined for all resolved NOE cross-peaks in a series of five NOESY spectra recorded under identical conditions. Distances were calculated from the initial slope of the build-up curves on the basis of calibration with known distances in regular secondary structural elements. The upper bound of the distance restraint was set to the calculated distance plus a correction factor of 10% to take into account remaining effects caused by internal motion and spin diffusion. For methyl groups, a correction of 0.3 Å was added to the upper bound prior to addition of the correction factor (*42, 43*). Where ambiguities existed in the assignment of NOEs yielding the restraints, the possible distances occurring as a consequence of the alternative assignments were treated as $(\sum r^{-6})^{-1/6}$ sum, as were distances determined for equivalent and nonstereospecifically assigned atoms (*44*). No build-up curves were calculated for overlapped peaks; instead the upper bound was set to 4.95 Å. All lower bounds were set to 1.8 Å.

$^3J_{H^N-H^\alpha}$ couplings were measured in a high-resolution COSY spectrum with a digital resolution after zero-filling of 0.47 Hz/point (experimental resolution 1.8 Hz/point) in the acquisition dimension, using the built-in function of FELIX 95, and were used for restraining dihedral angles according to the Karplus equation (*45*).

For $^3J_{H^N-H^\alpha} < 6$ Hz $\phi = -60 \pm 40°$ and $^3J_{H^N-H^\alpha} > 8$ Hz $\phi = -120 \pm 40°$. Intermediate couplings were not used as restraints during structure calculations.

$^3J_{H^\alpha-H^\beta}$ couplings were estimated in the same COSY spectrum and categorized as small, medium, or large coupling. Together with intensity information from H^α-H^β and H^N-H^β cross-peaks in an 80 ms NOESY spectrum, we identified χ_1 restraints and stereospecific assignments for H^β protons. Proline H^β protons could be stereospecifically assigned directly on the basis of the H^β-H^α cross-peak intensity in an 80 ms NOESY spectrum. Of the two β-protons in proline, $H^{\beta 3}$ is closer to H^α and thus gives rise to the stronger of the two cross-peaks. In a similar fashion, the side-chain terminal amide protons of aspargine and glutamine residues were stereospecifically assigned based on the $H^{\delta 22}$ proton being closer than the $H^{\delta 21}$ proton to the β-protons in an aspargine residue, and analogous in a glutamine residue the $H^{\epsilon 22}$ proton is closest to the γ-protons of the two terminal amide protons.

Distance and dihedral angle restraints were included in structure calculation using the program X-PLOR (*46*). The structure calculation was initialized by distance geometry embedding without metrization. On the embedded structures, restrained simulated annealing and simulated annealing refinement was performed (*47*).

After the first rounds of structure calculation, the preliminary structures were used to reduce the ambiguity of the NOE cross-peak assignments as well as assignment of previously unassigned peaks in the NOESY spectra. Averaging using $(\sum r^{-6})^{-1/6}$ sum produces loose restraints, often in which none of the individual components of the distance restraints are satisfied; therefore, it is important to resolve ambiguities when this is possible.

Several cycles of structure calculation and reassessment of ambiguous NOE restraints were performed until no further improvements could be made. This resulted in structures having low X-PLOR energy as well as good convergence to a single region of conformational space. We used the NOEVIO program (*48*) to identify additional stereospecific assignments for diastereotopic atoms showing significantly different NOE intensities to external spins by comparison to distances in intermediate structures. Hydrogen bond geometry in the intermediate structures was analyzed using the HBONDS program (*48*). Hydrogen bonds predicted from the calculated structures that corresponded to slow amide exchange were introduced as hydrogen bond restraints during the final structure calculations. Each hydrogen bond was introduced as a 2.0 ± 0.3 Å distance restraint between the hydrogen and the acceptor and a 3.0 ± 0.3 Å distance restraint between the donor and the acceptor.

During the process of structure determination, intermediate structures were analyzed with respect to energies, restraint violations, and distribution of dihedral angles using programs NOEVIO, ANGLES (*48*), and PROCHECK (*49*). The ensemble of 23 finally accepted structures were selected out of 100 calculated structures on the criteria that no distance or dihedral angle restraint was violated by more than 0.2 Å or 2°, respectively. For superposition of structures involving side-chain atoms, the positions of symmetry-related pairs of atoms ($C^{\delta 1}$/$C^{\delta 2}$ and $C^{\epsilon 1}$/$C^{\epsilon 2}$ of Tyr and Phe; $O^{\epsilon 1}$/$O^{\epsilon 2}$ of Glu; $O^{\delta 1}$/$O^{\delta 2}$ of Asp) were exchanged as needed to populate a unique dihedral rotomer using the program ANGLES (*48*). Superpositions and rmsd comparisons of structure ensembles were made with the POSER program using precision weights (*50*) which increases the contrast in rmsd per residue,

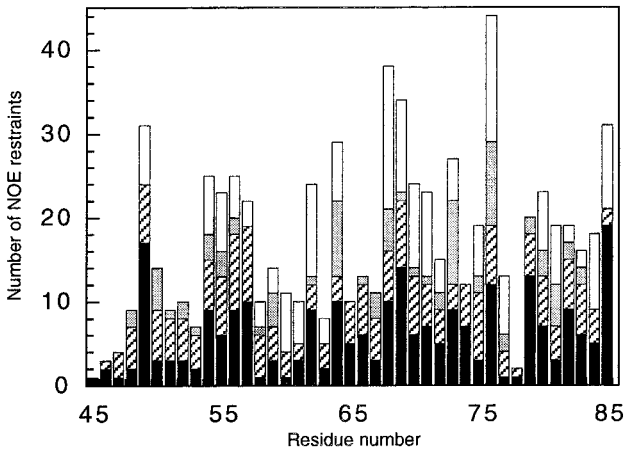

FIGURE 2: Graph indicating NOE-derived distance restraints per residue. Intraresidue NOEs are black, sequential NOEs are hatched, medium-range NOEs are gray, and long-range NOEs are white. In addition, 37 ambiguous NOE-derived distance restraints were used in the structure calculation.

compared to uniform weights, between well-defined and disordered regions without the need to preselect superposition residues.

RESULTS

Assignment. Complete sequence-specific ^{1}H assignments were made for synthetic FVII EGF1 with the exception of labile protons which undergo rapid exchange (Table S1, Supporting Information). In the case of Pro^{54} and Pro^{74}, the $d_{\alpha\delta(i-1,i)}$ NOE is clearly seen, while the $d_{\alpha\alpha(i-1,i)}$ NOE is absent, which indicates that the peptide bond preceding both prolyl rings are in the trans conformation (*39*). On the basis of the $^3J_{H^N-H^\alpha}$ and $^3J_{H^\alpha-H^\beta}$ coupling constants, as explained in the Material and Methods section, 14 ϕ and 5 χ_1 angle restraints could be included in the structure calculations.

By evaluating $^3J_{H^\alpha-H^\beta}$ coupling constants and H$^\alpha$-H$^\beta$ and H^N-H$^\beta$ NOE cross-peaks, the H$^\beta$-protons of Phe^{76} and Lys^{85} could be stereospecifically assigned. On the basis of relative NOE intensities, the stereospecific assignments of the H$^\beta$-protons of Pro^{54} and all side-chain terminal amide protons except those of Gln^{66} could be made. Analysis of the accepted structures after preliminary rounds of structure calculation yielded further stereospecific assignments of eight H$^\beta$-proton pairs, the H$^\alpha$-protons of Gly^{59} and the methyl groups of Leu^{73}. In the final calculation, six hydrogen bonds were included (Table S2, Supporting Information).

Structure. A total of 546 restraints was used for the structure calculation, including 521 NOE derived distance restraints distributed as 248 intraresidue ($j = i$), 98 sequential ($j = i + 1$), 43 medium range ($j = i + 2$,3, or 4), and 95 long range ($j > i + 4$) (Figure 2). A total of 37 ambiguous distance restraints remained in the final restraint set and could not be resolved on the basis of the final structures, possibly due to contributions from several pairs of protons to the measured NOE intensity. The remaining restraints were distributed as 14 ϕ and 5 χ_1 angle restraints and six hydrogen bond restraints. Nineteen diastereotopic centers were stereospecifically assigned prior to the final structure calculation.

The salient features of the tertiary structure (Figure 3) are two antiparallel β-sheets, one major β-sheet comprising residues Ser^{60}−Asp^{63} and Tyr^{68}−Phe^{71}, and a smaller one

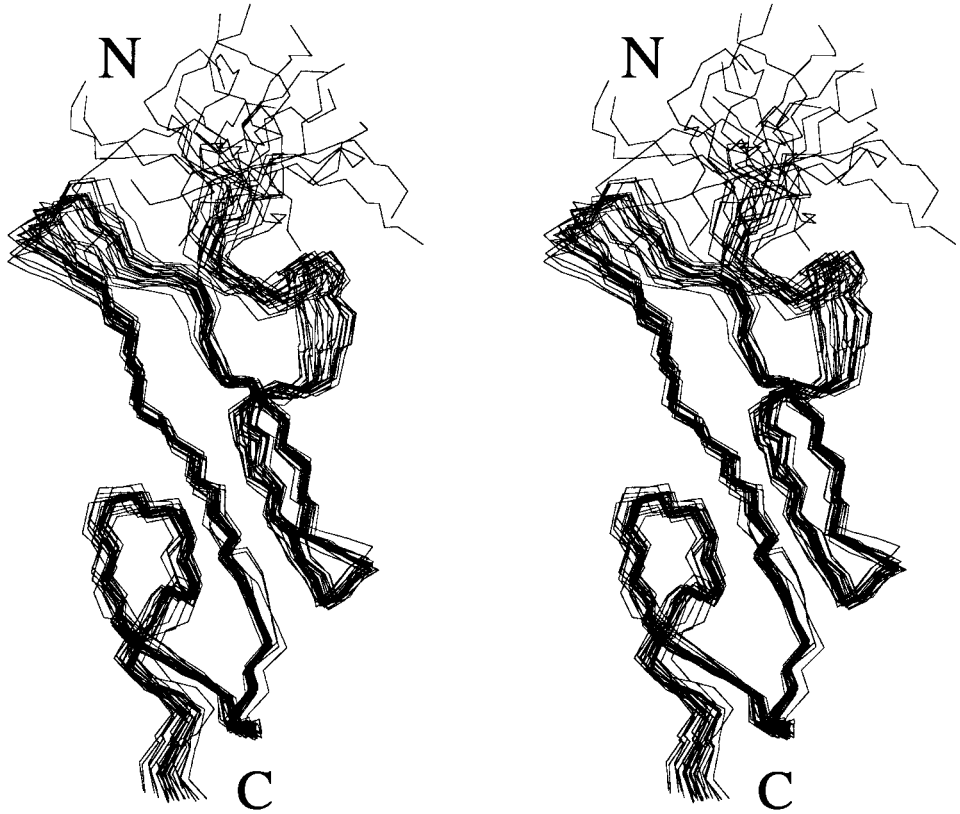

FIGURE 3: Stereoview of the 23 accepted structures of FVII EGF1. Shown is a precision-weighted superposition of backbone atoms (N, C$^\alpha$, C) for all residues (45−85) made using the POSER program. This figure was generated with a locally modified version of MOLSCRIPT, v1.1 program (*75*).

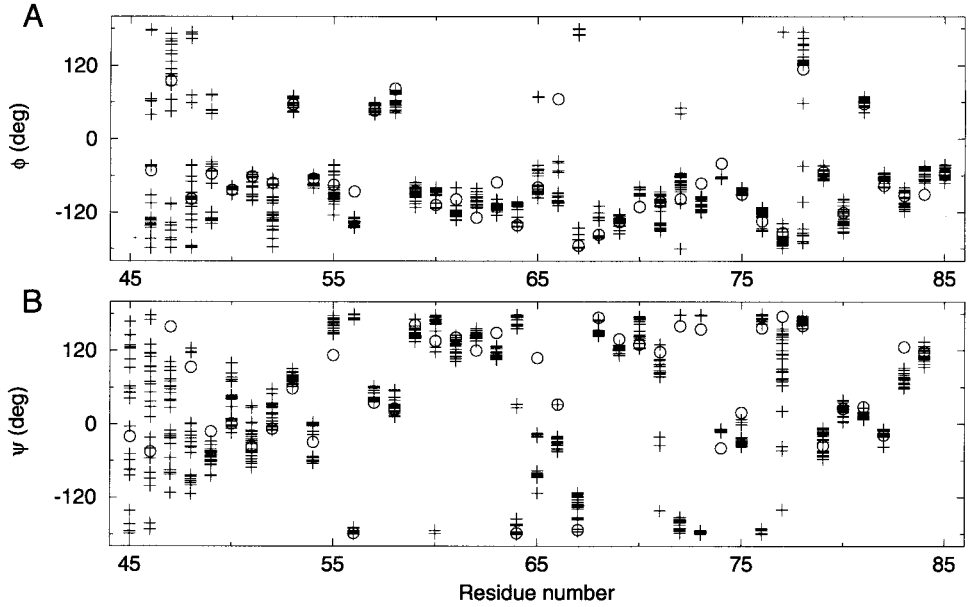

FIGURE 4: Graph demonstrating the ϕ angles (A) and ψ angles (B) for each residue. Angles of each of the 23 final NMR structures are represented as plus signs and angles of the crystal complex are represented as a circle.

involving residues Phe[76]−Glu[77] and Thr[83]−His[84]. Moreover, the N-terminal half of FVII EGF1 is connected to the C-terminal half by several NOEs between residues Pro[54]−Asn[57] on one hand and residues Asn[80]−Cys[81] on the other hand. The major β-sheet is preceded by two turns where residues 50−53 form a type I turn and residues 56−59 form a type I′ turn (*51, 52*). The first strand of the major β-sheet is brought back to the second strand by an irregular turn comprising residues 64−67. After the second strand of the major β-sheet, the peptide chain continues into a type I turn, consisting of residues 73−76, which is succeeded by the minor β-sheet where the two strands are connected by a type I turn made up by residues 78−81. Residues Cys[81]−Glu[82], which precede the last strand of the minor β-sheet, form a β-bulge, characterized by a hydrogen bond from Cys[81] H^N to Gly[78] O. A β-bulge, either of the same type as in FVII EGF1 or of the S3 class, has been found in this position in several homologous domains (*53*). All three disulfide bonds are a mixture of left- and right-handed conformations.

No interresidue NOEs were found to the four most N-terminal residues (Ser[45]−Asp[48]), and as a result, this part of the domain is poorly defined in the structure. We believe that this is an effect of having an isolated EGF1 domain lacking the N-terminal Gla domain which precedes EGF1 in the intact protein. Also, the absence of a Ca^{2+} ion in the EGF1 site contributes to the apparent disorder in this part of the molecule. Similar results were reported for the previously determined structures of homologous domains (*27, 54, 55*). For the residues 49−84, we have calculated the rmsd to the average structure to 0.54 Å for the backbone atoms (N, C^α, C) and 1.04 Å for all heavy atoms. For the same residues, 98% of the backbone dihedral angles (Figure 4) fall within the allowed regions according to PROCHECK (*49*). The corresponding rmsd numbers for the N-terminal part of the protein, residues 49−73, are 0.50 and 0.93 Å. For the C-terminal part, residues 74−84, the rmsd is 0.29 and 1.06 Å. A statistical summary of conformational energies and rmsds for the accepted structures is presented in Table 1.

Table 1: Statistical Summary of Average Conformational Energies and rmsds for the 23 Accepted Structures of FVII EGF1

energy (kcal mol^{-1})	
total	70.4 ± 7.9
bonds[a]	2.48 ± 0.37
angles	46.1 ± 3.4
impropers	6.20 ± 0.36
van der Waals[b]	5.31 ± 2.15
NOE restraints[c]	10.2 ± 2.6
dihedral restraints	0.140 ± 0.068
rmsd from experimental restraints	
NOE distance restraints (Å)	0.0194 ± 0.0025
dihedral angle restraints (deg)	0.337 ± 0.087
rmsd from ideal covalent geometry	
bonds (Å)	0.0021 ± 0.0002
angles (deg)	0.539 ± 0.020
impropers (deg)	0.366 ± 0.010

[a] Idealized covalent geometry and force constants are defined by the X-PLOR parameter file "parallhdgnew.pro" (*46*). [b] For the van der Waals function a simple repulsive energy term was used. [c] A square-well potential with force constants of 50 kcal mol^{-1} $Å^{-2}$ and 200 kcal mol^{-1} rad^{-2} for NOE and dihedral angle potentials, respectively, was used for the final calculations.

DISCUSSION

Comparison with the Corresponding Part of the X-Ray Structure of the Complex between TF and FVII. We have compared the structure of apo FVII EGF1 in solution to the corresponding domain in the X-ray structure of the complex between FVIIa and TF, where one Ca^{2+} ion is bound to the N-terminal EGF-like domain (PDB code 1dan) (*17*).

The protein backbones are similar with the exception of the first few N-terminal residues, which are flexible in the solution structure, and a small stretch around Gln[66] which will be discussed below. The average rmsd between the 23 NMR structures and the X-ray structure is 1.10 Å for backbone atoms (N, C^α, C) in residues 49−84. Calculation of precision-weighted rmsd per residue for the 23 NMR structures and the X-ray structure versus the average NMR structure reveals significant differences (larger than two standard deviations) for residues Ser[52], Lys[62], Gln[66], and Ser[67] and smaller but still significant deviations for Cys[70], Cys[72],

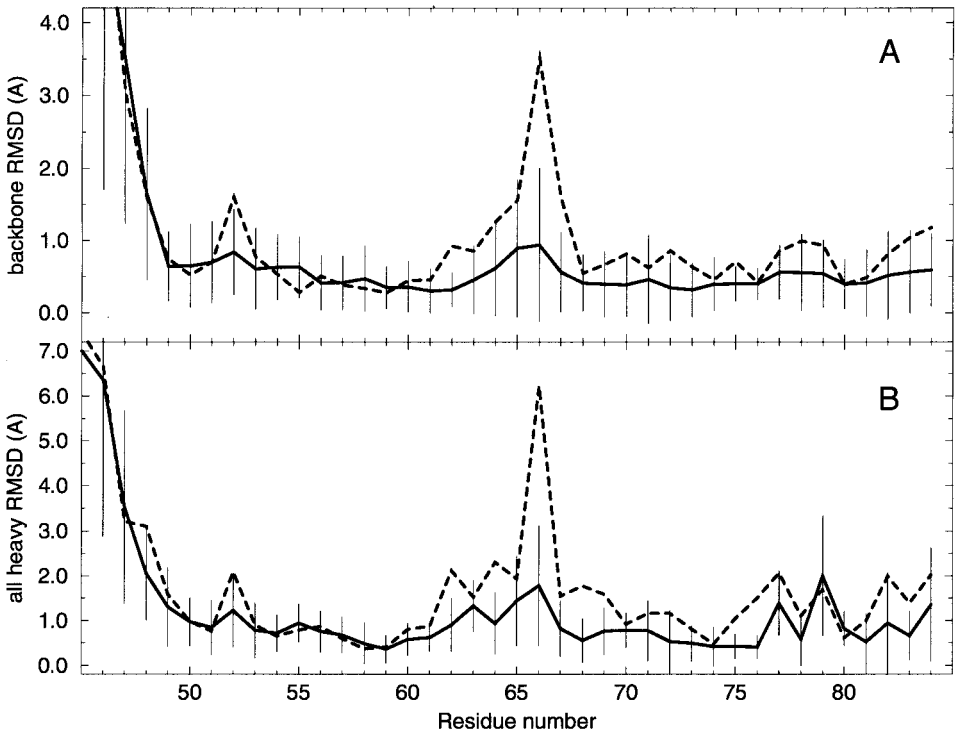

FIGURE 5: The solid line shows the precision weighted rmsd for the 23 accepted NMR structures versus the average structure with error bars indicating two standard deviations. The dashed line corresponds to the precision weighted rmsd between the X-ray structure and the average NMR structure. Backbone atoms (N, C^{α}, C) (A) and all heavy atoms (B).

Ala[75], and His[84] (Figure 5A). An alternative way of comparing structures is to calculate a distance difference matrix (*56, 57*). We calculated a distance difference matrix of average intramolecular $C^{\alpha}-C^{\alpha}$ distances using the program DISCOM (*48*). The matrix (Figure 6) reveals that a short stretch of residues centered around Gln[66] are closer to the N-terminal region (residues 46−60) in the crystal structure than in the NMR structures. This may be due to an effect of Ca^{2+} ligation as nearby residues Asp[63] and Gln[64] approach remaining ligands Asp[46], Gly[47], and Gln[49]. Particularly, the shorter distance between Asp[63] and Gln[64] on one hand and Gln[49] on the other hand would support such an argument. However, Gln[66], which is part of the turn connecting the two strands of the major β-sheet, is in the center of a three residue stretch of residues lacking long-range distance restraints (Figure 2). As a consequence this region, is underdetermined in the NMR structures and conclusions have to be drawn with caution. Other notable differences between the structures are found for the distances between residues 60−63 and 69−74 on one hand and the most C-terminal turn of the domain involving residues 78−79 on the other hand. These distances are shorter in the NMR structures than in the crystal structure. Again, caution has to be taken in the interpretation as residues 78−79 lack long-range NOEs. A comparison of backbone dihedral angles in the NMR structures and the X-ray structure (Figure 4) also reveals a high degree of similarity with the exception of the most N-terminal residues which are disordered in the NMR structures. However, in three cases (residues 55−56, 65−66, and 83−84), we observe a rotational displacement of the peptide plane about the $C^{\alpha}_{i-1}-C^{\alpha}_{i}$ virtual bond characterized by anticorrelated ψ_{i-1}, ϕ_i dihedral angles. The largest effect is seen for the peptide plane between Leu[65] and Gln[66], which is in the three residue stretch described above. The $^3J_{H^N-H^{\alpha}}$ coupling constant for Gln[66] is 7.9 Hz, which is close to the cut off ($^3J_{H^N-H^{\alpha}} > 8$ Hz) used to produce a ϕ angle restraint of $-120 \pm 40°$. Uncertainty in the calibration of the Karplus curve (*45*) and in the coupling measurement yield degenerate solutions for ϕ near −120 and +65°, the latter of which is adopted by the crystal structure. In our structures, this unrestrained ϕ angle varies between −36 and −104°. With the exception of Gln[66], the angle comparison (Figure 4) shows a high correspondence of residues with positive ϕ angles in the solution and the crystal structures, although no explicit positive ϕ restraints were applied during the structure calculation.

When the precision-weighted rmsd per residue is calculated including all heavy atoms, the same trend as for the backbone atoms emerge (Figure 5B). Alanine-scanning mutagenesis identified Gln[64], Ile[69], Phe[71], and Arg[79] and three residues in the protease domain as important for TF binding (*18*). In the structure of the complex, it was demonstrated that Ile[69], Phe[71], and Arg[79] played a crucial role for binding by providing the major hydrophobic interaction with TF. Arg[79] makes several hydrogen bonds to TF and is important for binding as revealed by studies of a naturally occurring mutant where this residue was replaced by a glutamine (*58*). We have found that these side chains in the solution structure are located in approximately the same orientations as in the complex (Figure 7). For Ile[69] and Phe[71] the positions of the side chains in the crystal structure correspond roughly to the outer perimeter of the NMR ensemble, while Arg[79] is centered in the NMR ensemble. Several intermolecular hydrogen bonds were reported between residues in EGF1 and TF. Most of these residues have the same orientation in the solution structure of the isolated EGF1 domain. The exceptions are Glu[77], where the side-chain position in the crystal structure superpose to the perimeter of the solution structure ensemble, and Gln[64], where both the χ_1 and χ_2 angles differ and the χ_3 angle is disordered in the NMR

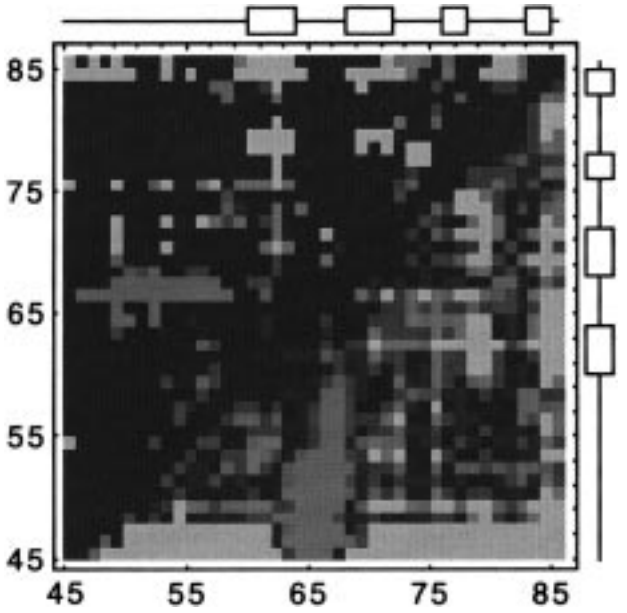

FIGURE 6: Graphical representation of a distance difference matrix containing the average distance differences between $C^{\alpha}-C^{\alpha}$ distances in the 23 final NMR-derived structures of FVII EGF1 and the corresponding part of the crystal complex. The lower right half of the matrix shows all differences while the upper left half shows only significant differences (larger than 2 standard deviations). The differences are color coded in a linear RGB (red, green, blue) scale from cyan to magenta. Cyan (0, 1, 1) corresponds to distance differences of 1 Å or larger positive values and magenta (1, 0, 1) to −1 Å or larger negative values. If there is no difference between the $C^{\alpha}-C^{\alpha}$ distances in the NMR compared to the corresponding distance in the crystal structure, the matrix element is colored blue (0, 0, 1). Thus, an element colored in cyan indicates that the corresponding distance is longer in the crystal structure than in the NMR structures, while a magenta-colored matrix element indicates the reverse. The maximum distance differences (excluding the disordered four N-terminal and one C-terminal residue) are 2.02 Å ($Lys^{62}-Arg^{79}$) and −4.20 Å ($Ser^{52}-Gln^{66}$). On top and to the right of the matrix the secondary structure of the protein is indicated. The boxes represent the strands of the β-sheets and a line represents all other parts of the protein (turn region or region with no regular secondary structure). The matrix was plotted using Mathematica (Wolfram Research).

structures. Also, the cavity close to the Cys^{72} to Cys^{81} disulfide bridge, where Lys^{20} of TF interacts with FVII, is located in the same position in the two structures. The Ca^{2+} ion is ligated by Asp^{46} $O^{\delta 2}$, Gly^{47} O, Gln^{49} $O^{\epsilon 1}$, Asp^{63} $O^{\delta 1}$, Asp^{63} $O^{\delta 2}$, and Gln^{64} O. As mentioned, the N-terminal residues ($Ser^{45}-Asp^{48}$) are poorly defined in the NMR structures. A comparison of the location of the remaining Ca^{2+} ligands in the Ca^{2+}-free solution structure and the Ca^{2+}-bound crystal structure reveals that the side chain of Gln^{49} has the same direction, although a considerable spread. Gln^{64} O and Asp^{63} C^{β} are in the same position as in the crystal structure; however, the χ_1 angle of Asp^{63} is disordered. As mentioned, the side chain of Gln^{64}, which makes a hydrogen bond to Gln^{110} in TF in the complex structure, is disordered. However, mutational studies have shown that the effect on the complex formation by the $Gln^{110} \rightarrow$ Ala mutation is additive to the effect caused by the $Asp^{63} \rightarrow$ Ala mutation; therefore, it is not likely that the conformational change of the Gln^{64} side chain is responsible for the reduction in TF affinity for the Ca^{2+}-free FVIIa as compared to FVIIa with Ca^{2+} in the EGF1 site (*19*).

When the solution structures of the Ca^{2+}-loaded and Ca^{2+}-free EGF1 domains from FX were compared, it was reported that in the Ca^{2+}-loaded structure the major β-sheet moves closer to the N-terminal part, and both of these parts of the structure become better defined. The structural change was also accompanied by amide proton shift changes for some of the Ca^{2+}-ligating residues and some other residues near to the Ca^{2+}-binding site. Notably, among the nonligating residues that displayed large shift changes were residues 51−52 and 65−66 (the numbering of FX and FVII is coincident) (*54*). In our comparison of solution and crystal structures of FVII EGF1, residue 52 and 66 are significantly different judging from precision-weighted rmsd measurements and for the latter also from the distance difference matrix. Also, for the EGF-like domain of C1r, shift changes were reported for non-Ca^{2+}-ligating residues in the turn region upon Ca^{2+} binding (*53*). To further put our observations in perspective, we compared the NMR structure of an isolated domain of apo human FIX EGF1 (*34*) to the crystal structure of an isolated domain of Ca^{2+}-bound human FIX EGF1 (*55*) and the crystal structure of intact porcine FIX lacking Ca^{2+} in the EGF1 site (*59*). These comparisons show the same trend as our observations for FVII with regard to distance differences for the sequence range 63−67 (FVII numbering) versus the N-terminal part of the protein. This raises the possibility that differences could, in part, be due to other factors than Ca^{2+} binding.

Our comparison of the structure of residues involved in FVIIa binding to TF suggests that the interaction surface on FVII EGF1 is preformed for binding to TF independently of binding of Ca^{2+} to the EGF-like domain.

In the TF:FVIIa complex, the side-chain oxygen of Gln^{64} was reported to form a hydrogen bond to Gln^{110} in TF. Other than that, the residues important for TF binding are located away from the Ca^{2+} site, and it is hard to imagine that the small local changes mentioned above can have a direct implication on the ability of FVIIa to bind TF. Still, we know that the Ca^{2+}-binding site is essential for complex formation. It has been shown for a Gla-EGF1 pair from FX that the relative orientation between the two domains change upon Ca^{2+} binding to the EGF1 domain (*27*). Mutational studies on FVII have shown that mutations of Ca^{2+}-ligating residues lead to impaired TF binding. It was also shown that this effect is additive to the effect caused by a mutation of a residue in the interaction surface, either in FVII or in TF, suggesting that the impairment of binding due to mutations in the Ca^{2+}-binding site on one hand and of interaction surface residues on the other hand are independent of one another (*19*). All of these observations support the hypothesis that Ca^{2+} binding to the EGF-like domain is important for rearranging and stabilizing the relative position of the N-terminal EGF-like domain with respect to the Gla domain and thereby facilitating binding to TF, rather than initiating a local conformational change in the N-terminal EGF-like domain. This hypothesis can now be strengthened as the comparison of the structure in this work with the TF:FVIIa complex does not reveal any major conformational changes of the interaction surface.

Comparison with $Asn^{57} \rightarrow Asp$ Mutant. It has been reported that the naturally occurring mutant $Asn^{57} \rightarrow$ Asp does not bind to TF as a result of misfolding of the EGF1 domain due to the inability to form the hydrogen bond

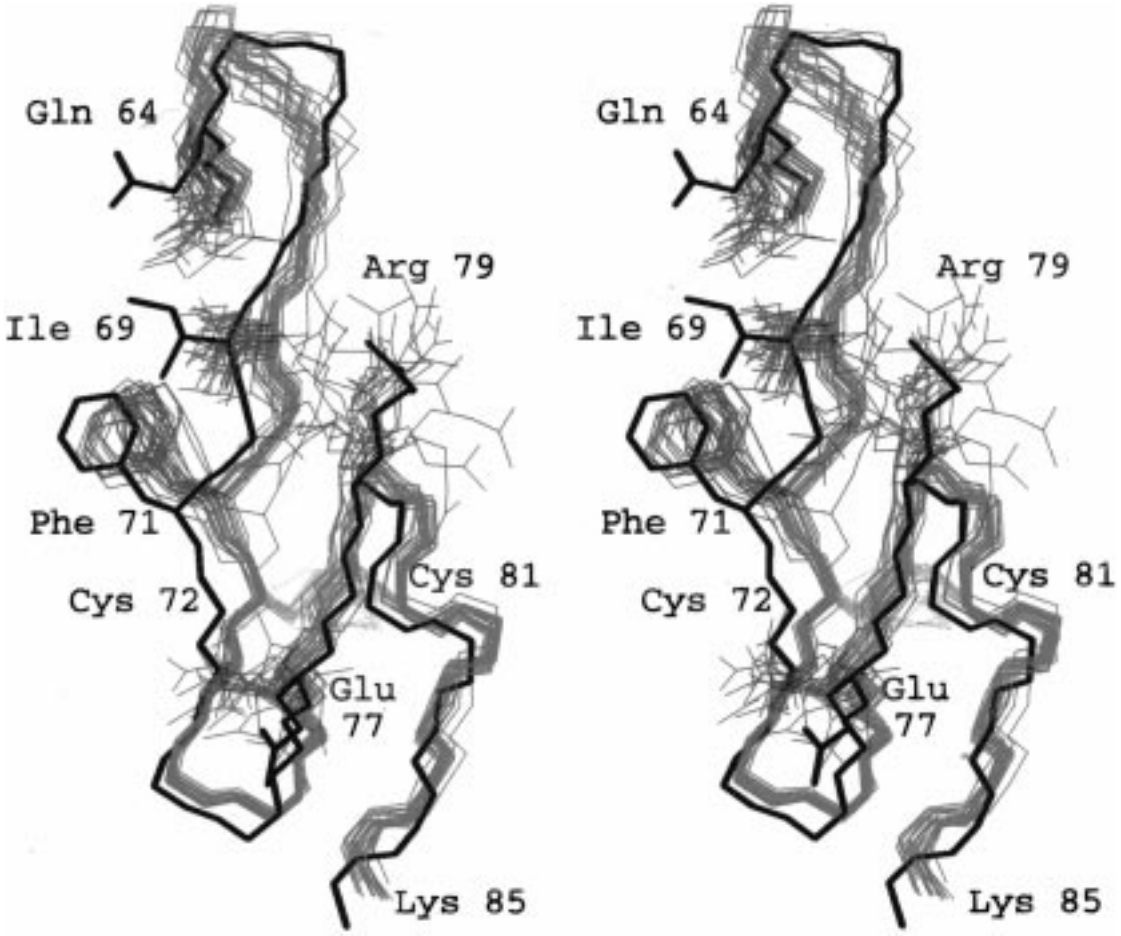

FIGURE 7: Stereo representation of the backbone trace of residues 63−85 and side-chain heavy atoms of residues Gln[64], Ile[69], Phe[71], Glu[77], Arg[79], Cys[72], and Cys[81], the latter two constituting the 5−6 disulfide bond. The ensemble of 23 accepted NMR structures is magenta (backbone trace), cyan (side chains), and yellow (disulfide bond 5−6), and the crystal structure (PDB code 1dan) black. Backbone atoms (N, C^{α}, C) of all residues (45−85) were used for precision-weighted superposition using the program POSER. The displayed side chains have been pointed out on structural and biochemical grounds as being important for interaction with TF. This figure was generated with the program MOLMOL (*76*).

between Asp[57] $N^{\delta 2}$ and Cys[81] O (*60*). In the crystal structure, the distance between these atoms is 2.83 Å, indicating that a hydrogen bond is formed. In our structures, we see significant variation of this distance (3.22 ± 0.61 Å), although most structures have a donor−acceptor distance compatible with a hydrogen bond. However, the angle defined by donor-hydrogen and hydrogen-acceptor vectors lies near 90° for both protons while a value in the range 135−180° would be expected for a hydrogen bond (*61*). As a consequence, the proton-acceptor distances are longer (3.10 ± 0.55 and 3.11 ± 1.10 Å for $H^{\delta 21}$ and $H^{\delta 22}$ to the acceptor, respectively) than anticipated for a N−H···O═C hydrogen bond (2.00 ± 0.01) (*61*). We believe this to be an effect of the absence of attractive electrostatic or van der Waals terms used in the structure calculations. In exchange experiments, Asp[57] $H^{\delta 22}$ is exchanging slowly, while the exchange rate of Asp[57] $H^{\delta 21}$ cannot be determined due to overlap. A slow amide proton exchange rate as determined by NMR indicates that the amide is involved in a hydrogen bond, but there is no way of identifying the acceptor with this technique. To test whether the structures would accommodate a hydrogen bond in this position two new structure calculations were performed where we included a hydrogen bond restraint from either Asn[57] $H^{\delta 21}$ or $H^{\delta 22}$ to Cys[81] O. The latter calculation yielded energies on the same level or lower, while the former yielded energies slightly (4−10 kcal/mol) above our original calculations. We believe that the presence of the Asn[57] $N^{\delta 2}$ to Cys[81] O hydrogen bond, important for the tertiary fold of the domain, is consistent with the NMR structures although they are not proven.

Comparison with Homologous Proteins. FVII EGF1 has a high degree of sequence similarity with the corresponding domain in FIX and FX, with a sequence identity of 61% for human factor IX and 49% for bovine factor X (Figure 8). We have assigned the ^{1}H NMR resonances from FVII EGF1 and compared the secondary chemical shifts (*62*) of backbone amide protons and the H^{α}-protons with the shifts from the corresponding Ca^{2+}-free N-terminal EGF-like domains from FIX (*63*) and bovine FX (*64*) (Figure S2, Supporting Information). This comparison revealed a striking similarity for all three domains. As the chemical shift to a high extent is determined by the local environment of the spin, this implies that the structures of these domains must be similar (Figure 9). It is, however, not apparent from the secondary shift comparison that either of the three EGF1 modules is more similar to any one other.

The pairwise rmsd of the 23 accepted structures of FVII EGF1 and the 13 deposited structures of FX EGF1 is 1.52 ± 0.16 Å for backbone atoms (N, C^{α}, C) of residues 49−84. The most apparent difference is that the distance between

```
hFVII EGF1   SDGDQC ASSPCQNGGS CKDQLQSYIC FCLPAFEGRN CETHK
hFIX EGF1   YVDGDQC ESNPCLNGGS CKDDINSYEC WCPFGFEGKN CELDVT
bFX EGF1     KDGDQC EGHPCLNQGH CKßGIGDYTC TCAEGFEGKN CEFSTR
              45   50    55   60    65   70    75   80    85
```

FIGURE 8: Alignment of the primary sequence of the N-terminal EGF-like domain (EGF1) in human FVII, human FIX and bovine FX. Disulfide bonds are indicated by lines. Residue 63 in FX EGF1 is *erythro*-β-hydroxyaspartic acid, formed by postribosomal hydroxylation of an aspartic acid. In human FIX this residue is 30% hydroxylated, while in human FVII it is not hydroxylated at all. The sequences are aligned according to FVII numbering (same as FX numbering). Addition of 1 to the residue number gives the FIX numbering.

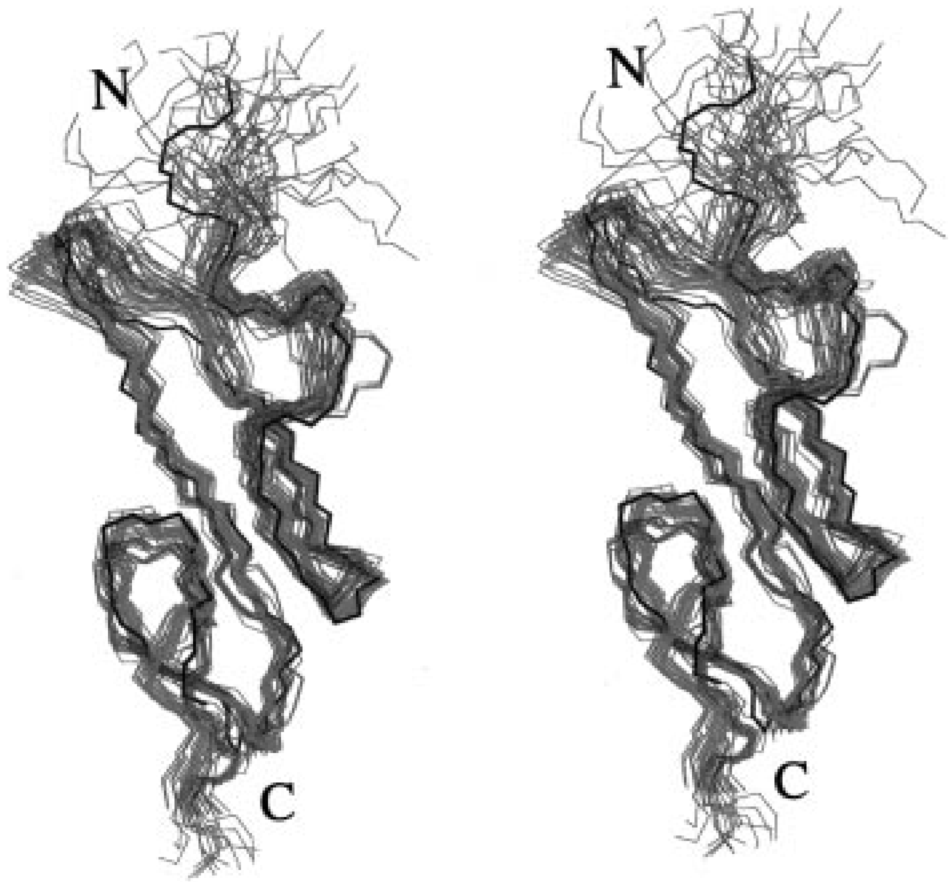

FIGURE 9: Stereoview of the structures of EGF1 domains from the homologous clotting factors VII (magenta, 23 structures), IX (black, minimized average structure PDB code 1ixa) and X (cyan, 13 structures PDB code 1apo). Shown is a precision-weighted superposition of backbone atoms (N, C^{α}, C) for all residues (45−85) made using the POSER program. The orientation of the molecules in this figure is the same as in Figure 3. This figure was generated with a locally modified version of MOLSCRIPT, v1.1 program (*75*).

the most C-terminal turn (residues 78−81) and last strand (residues 83−84) on one hand and the major β-sheet on the other hand is shorter in FVII than in FX. However, the orientation of the C-terminal part of the molecule (residues 75−85) relative to the rest of the molecule is not very well determined in FVII structures due to a limited number of long-range NOE restraints to that region.

FIX EGF1 is more similar to FVII EGF1 in amino acid sequence (Figure 8). The rmsd for the 23 FVII EGF1 structures to the minimized average structure of FIX EGF1 is 1.16 ± 0.07 Å for backbone atoms (N, C^{α}, C) of residues 49−83 (FVII numbering). The most significant dissimilarity between FIX and FVII structures is, again, a tighter packing of the C-terminal loop to the rest of the molecule in FVII. In addition, the turn at residues 73−75 is structurally different as the sequence Leu^{73}-Pro^{74}-Ala^{75}-Phe^{76} is replaced by Pro^{73}-Phe^{74}-Gly^{75}-Phe^{76} (FVII numbering) in FIX. This turn is of type I in FVII while, in both FIX and FX, it is a type II turn (*51,52*).

The chemical shift of the amide proton of the residue corresponding to Glu^{82} has been reported to be downfield of 9.6 ppm in several NMR studies of EGF-like domains from other proteins (*34, 63−69*). In our study, this shift is at 10.38 ppm and the amide proton is exchanging slowly. It has been suggested that this unusual chemical shift is a consequence of the amide forming a hydrogen bond to its own side-chain carboxylate (*65*). We measured the possible donor-acceptor as well as the hydrogen-acceptor distances in our structures but found no evidence of a hydrogen bond. However, as discussed above, there was no driving force included in the structure calculation to encourage the formation of hydrogen bonds. In the crystal structure of the

TF:FVIIa complex, the Glu^{82} N to Glu^{82} $O^{\epsilon 1}$ distance is 2.66 Å and thus indicative of a hydrogen bond. In homologous domains, hydrogen bonds have been found in crystal structures, FIX EGF1 (*59*) and E-selectin (*70*), while they have been absent in solution structures, FIX EGF1 (*34*), FX EGF1 (*71*), TGF-α (*72*), hEGF (*67*), u-PA (*68*), and t-PA (*73*). A recent NMR study of the EGF-like domain from the complement protease C1r (*53*) also reveals a strongly downfield shifted amide proton resonance, although at a slightly different position, which is structurally homologous to the EGF2 domains of FIX (*59*) and FX (*74*).

ACKNOWLEDGMENT

We thank Ingrid Dahlquist for synthesising the FVII EGF1 domain.

SUPPORTING INFORMATION AVAILABLE

Table S1, ^1H chemical shifts; Table S2, the hydrogen bonds observed in the final structures; Figure S1, the fingerprint region of a TOCSY spectrum; Figure S2, a comparison of H^N and H^α secondary chemical shifts of EGF1 domains from FVII, FIX and FX (5 pages). Ordering information is given on any current masthead page.

REFERENCES

1. Brooze, G. J., and Majerus, P. W. (1980) *J. Biol. Chem. 255*, 1242−1247.
2. Bajaj, S. P., Rapaport, S. I., and Brown, S. F. (1981) *J. Biol. Chem. 256*, 253−259.
3. Petersen, L. C., Valentin, S., and Hedner, U. (1995) *Thromb. Res. 79*, 1−47.
4. Fair, D. S. (1983) *Blood 62*, 784−791.
5. Wildgoose, P., Nemerson, Y., Hansen, L. L., Nielsen, F. E., Glazer, S., and Hedner, U. (1992) *Blood 80*, 25−28.
6. Morrisey, J. H., Macik, B. G., Neuenschwander, P. F., and Comp, P. C. (1993) *Blood 81*, 734−744.
7. Howard, P. R., Bovil, E. G., Pike, J., Church, W. R., and Tracy, R. P. (1994) *Thromb. Haemost. 72*, 21−27.
8. Nemerson, Y. (1988) *Blood 71*, 1−8.
9. Camerer, E., Kolstø, A.-B., and Prydz, H. (1996) *Thromb. Res. 81*, 1−41.
10. Harlos, K., Martin, D. M. A., O'Brien, D. P., Jones, E. Y., Stuart, D. I., Polikarpov, I., Miller, A., Tuddenham, E. G. D., and Boys, C. W. G. (1994) *Nature 370*, 662−666.
11. Muller, Y. A., Ultsch, M. H., Kelly, R. F., and DeVos, A. M. (1994) *Biochemistry 33*, 10864−10870.
12. Hagen, F. S., Gray, C. L., O'Hara, P., Grant, F. J., Sarri, G. C., Woodbury, R. G., Hart, C. E., Insley, M., Kisiel, W., Kurachi, K., and Davie, E. W. (1986) *Proc. Natl. Acad. Sci. U.S.A. 83*, 2412−2416.
13. Bauer, K. A. (1997) *Thromb. Haemost. 78*, 108−111.
14. Davie, E. W., Fujikawa, K., and Kisiel, W. (1991) *Biochemistry 30*, 10363−10370.
15. Rapaport, S. I., and Rao, L. V. M. (1995) *Thromb. Haemost. 74*, 7−17.
16. Martin, D. M. A., Boys, C. W. G., and Ruf, W. (1995) *FASEB J. 9*, 852−859.
17. Banner, D. W., D′Arcy, A., Chène, C., Winkler, F. K., Guha, A., Konigsberg, W. H., Nemerson, Y., and Kirchhofer, D. (1996) *Nature 380*, 41−46.
18. Dickinson, C. D., Kelly, C. R., and Ruf, W. (1996) *Proc. Natl. Acad. Sci. U.S.A. 93*, 14379−14384.
19. Kelly, C. R., Dickinson, C. D., and Ruf, W. (1997) *J. Biol. Chem. 272*, 17467−17472.
20. Banner, D. W. (1997) *Thromb. Haemost. 78*, 512−515.
21. Kirchhofer, D., and Banner, D. W. (1997) *Trends Cardiovasc. Med. 7*, 316−324.
22. Sabharwal, A. K., Birktoft, J. J., Gorka, J., Wildgoose, P., Petersen, L. C., and Bajaj, S. P. (1995) *J. Biol. Chem.* 15523−15530.
23. Schiødt, J., Harrit, N., Christensen, U., and Petersen, L. C. (1992) *FEBS Lett. 306*, 265−268.
24. Wildgoose, P., Foster, D., Schiødt, J., Wiberg, F. C., Birktoft, J. J., and Petersen, L. C. (1993) *Biochemistry 32*, 114−119.
25. Persson, E., Olsen, O. H., Østergaard, A., and Nielsen, L. S. (1997) *J. Biol. Chem. 272*, 19919−19924.
26. Banner, D. W. (1997) *XVIth Congress of the International Society on Thrombosis and Haemostasis*
27. Sunnerhagen, M., Olah, G. A., Stenflo, J., Forsén, S., Drakenberg, T., and Trewhella, J. (1996) *Biochemistry 35*, 11547−11559.
28. Bjoern, S., Foster, D. C., Thim, L., Wiberg, F. C., Christensen, M., Komiyama, Y., Pedersen, A. H., and Kisiel, W. (1991) *J. Biol. Chem. 266*, 11051−11057.
29. Thim, L., Bjoern, S., Christensen, M., Nicolaisen, E. M., Lund-Hansen, T., Pedersen, A. H., and Hedner, U. (1988) *Biochemistry 27*, 7785−7793.
30. Campbell, I. D., and Bork, P. (1993) *Curr. Opin. Struct. Biol.* 385−392.
31. Appella, E., Weber, I., and Blasi, F. (1988) *FEBS Lett. 231*, 1−4.
32. Engel, J. (1989) *FEBS Lett. 251*, 1−7.
33. Henikoff, S., Greene, E. A., Pietrokovski, S., Bork, P., Attwood, T. K., and Hood, L. (1997) *Science 278*, 609−614.
34. Baron, M., Norman, D. G., Harvey, T. S., Handford, P. S., Mayhew, M., Tse, A. G. D., Brownlee, G. G., and Campbell, I. D. (1992) *Protein Sci.* 81−90.
35. Aue, W. P., Bartholdi, E., and Ernst, R. R. (1976) *J. Chem. Phys. 64*, 2229−2246.
36. Braunschweiler, L., Bodenhausen, G., and Ernst, R. R. (1983) *Mol. Phys. 48*, 535−560.
37. Braunschweiler, L., and Ernst, R. R. (1983) *J. Magn. Reson. 53*, 521−528.
38. Macura, S., and Ernst, R. R. (1980) *Mol. Phys. 41*, 95−117.
39. Wüthrich, K. (1986) *NMR of Proteins and Nucleic Acids*, John Wiley & Sons, Inc., New York.
40. Chazin, W. J., Rance, M., and Wright, P. E. (1988) *J. Mol. Biol. 202*, 603−622.
41. Chazin, W. J., Rance, M., and Wright, P. E. (1988) *J. Mol. Biol. 202*, 623−636.
42. Konig, T. M. G., Boelens, R., and Kaptein, R. (1990) *J. Magn. Reson. 90*, 111−123.
43. Tropp, J. (1980) *J. Chem. Phys. 72*, 6035−6043.
44. Nilges, M. (1993) *Proteins: Struct., Funct., Genet. 17*, 295−309.
45. Pardi, A., Billeter, M., and Wüthrich. (1984) *J. Mol. Biol. 180*, 741−751.
46. Brünger, A. T. (1992) *X-PLOR version 3.1*, Yale University, New Haven, CT.
47. Nilges, M., Clore, M., and Gronenborn, A. M. (1988) *FEBS Lett. 229*, 317−324.
48. Gippert, G. P. (1995) Ph.D. Thesis, The Scripps Research Institute, La Jolla, CA.
49. Laskowski, R. A., MacArthur, M. W., Moss, D. S., and Thornton, J. M. (1993) *J. Appl. Crystallogr. 26*, 283−291.
50. Gippert, G. P., and Akke, M. (manuscript in preparation).
51. Chou, P. Y., and Fasman, G. D. (1977) *J. Mol. Biol. 115*, 135−175.
52. Richardson, J. S. (1981) *Adv. Protein Chem. 34*, 167−339.
53. Bersch, B., Hernandez, J.-F., Marion, D., and Arlaud, G. J. (1998) *Biochemistry 37*, 1204−1214.
54. Selander-Sunnerhagen, M., Ullner, M., Persson, E., Teleman, O., Stenflo, J., and Drakenberg, T. (1992) *J. Biol. Chem. 267*, 19642−19649.
55. Rao, Z., Handford, P., Mayhew, M., Knott, V., Brownlee, G. G., and Stuart, D. (1995) *Cell 82*, 131−141.
56. Nishikawa, K., Ooi, T., Isogai, Y., and Saito, N. (1972) *J. Phys. Soc. Jpn. 32*, 1331−1337.
57. Akke, M., Forsén, S., and Chazin, W. J. (1995) *J. Mol. Biol. 252*, 102−121.

58. O'Brien, D. P., Kemball-Cook, G., Hutchinson, A. M., Martin, D. M. A., Johnson, D. J. D., Byfield, P. G. H., Takamiya, O., Tuddenham, E. G. D., and McVey, J. H. (1994) *Biochemistry 33*, 14162−14169.
59. Brandstetter, H., Bauer, M., Huber, R., Lollar, P., and Bode, W. (1995) *Proc. Natl. Acad. Sci. U.S.A. 92*, 9796−9800.
60. Leonard, B. J. N., Chen, Q., Blajchman, M. A., Ofosu, F. A., Sridhara, S., Yang, D., and Clarke, B. J. (1998) *Blood 91*, 142−148.
61. Taylor, R., and Kennard, O. (1984) *Acc. Chem. Res. 17*, 320−326.
62. Merutka, G., Dyson, H. J., and Wright, P. E. (1995) *J. Biomol. NMR 5*, 14−24.
63. Huang, L. H., Cheng, H., Pardi, A., Tam, J. P., and Sweeney, W. V. (1991) *Biochemistry 30*, 7402−7409.
64. Selander, M., Persson, E., Stenflo, J., and Drakenberg, T. (1990) *Biochemistry 29*, 8111−8118.
65. Freedman, S. J., Sanford, D. G., Bachovchin, W. W., Furie, B. C., Baleja, J. D., and Furie, B. (1996) *Biochemistry 35*, 13733−13744.
66. Tappin, M. J., Cooke, R. M., Fitton, J. E., and Campbell, I. D. (1989) *Eur. J. Biochem. 179*, 629−637.
67. Hommel, U., Harvey, T. S., Driscoll, P. C., and Campbell, I. D. (1992) *J. Mol. Biol. 277*, 271−282.
68. Hansen, A. P., Petros, A. M., Meadows, R. P., Nettesheim, D. G., Mazar, A. P., Olejniczak, E. T., Xu, R. X., Pederson, T. M., Henkin, J., and Fesik, S. W. (1994) *Biochemistry 33*, 4847−4864.
69. Smith, B. O., Downing, A. K., Dudgeon, T. J., Cunningham, M., Driscoll, P. C., and Campbell, I. D. (1994) *Biochemistry 33*, 2422−2429.
70. Graves, B. J., Crowther, R. L., Chandran, C., Rumberger, J. M., Li, S., Huang, K.-S., Presky, D. H., Familletti, P., Wolitzky, B. A., and Burns, D. K. (1994) *Nature 367*, 532−538.
71. Ullner, M., Selander, M., Persson, E., Stenflo, J., Drakenberg, T., and Teleman, O. (1992) *Biochemistry 31*, 5974−5983.
72. Harvey, T. S., Wilkinson, A. J., Tappin, M. J., Cooke, R. M., and Campbell, I. D. (1991) *Eur. J. Biochem. 198*, 555−562.
73. Smith, B. O., Downing, A. K., Driscoll, P. C., Dudgeon, T. J., and Campbell, I. D. (1995) *Structure 3*, 823−833.
74. Padmanabhan, K., Padmanabhan, K. P., Tulinsky, A., Park, C. H., Bode, W., Huber, R., Blankenship, D. T., Cardin, A. D., and Kisiel, W. (1993) *J. Mol. Biol. 232*, 947−966.
75. Kraulis, P. J. (1991) *J. Appl. Crystallogr. 24*, 946−950.
76. Koradi, R., Billeter, M., and Wüthrich, K. (1996) *J. Mol. Graphics 14*, 51−55.

BI980522F